

Spatially inhomogeneous phase in the two-dimensional repulsive Hubbard model

Chia-Chen Chang and Shiwei Zhang

Department of Physics, College of William and Mary, Williamsburg, VA 23187

Using recent advances in auxiliary-field quantum Monte Carlo techniques and the phaseless approximation to control the sign/phase problem, we determine the equation of state in the ground state of the two-dimensional repulsive single-band Hubbard model at intermediate interactions. Shell effects are eliminated and finite-size effects are greatly reduced by boundary condition integration. Spin-spin correlation functions and structure factors are also calculated. In lattice sizes up to 16×16 , the results show signal for phase-separation. Upon doping, the system separates into one phase of density $n = 1$ (hole-free) and the other at density n_c (~ 0.9). The long-range antiferromagnetic order is coupled to this process, and is lost below n_c .

PACS numbers: 71.10.Fd, 02.70.Ss

I. INTRODUCTION

The Hubbard model¹ provides a minimal framework for describing electron interactions in a crystal lattice, and has played a central role in condensed matter and quantum many-body physics. Especially since the discovery of high- T_c superconductors, the two-dimensional (2-D) Hubbard model, believed to contain the essential physics of the CuO plane², has been intensely studied. The combination of theoretical and numerical techniques has made important progress^{3,4}, but some basic questions have remained.

One of the questions is whether there is phase separation (PS) in the ground state of the Hubbard model. The question is important in its own right, as a key element in our understanding of the phase diagram of this fundamental model. Recent experimental indication of spatial inhomogeneities in cuprates⁵ has further increased its potential relevance and interest. In the past two decades a large body of numerical work has been devoted to resolving this issue^{6,7,8,9,10,11,12,13,14}, but the results have been conflicting. The differing answers underscore the challenges: the requirement of high accuracy, as well as the difficulty in extrapolating to the thermodynamic limit because of extreme sensitivity of the signal to both finite-size and shell effects.

In this paper, we apply recent advances in auxiliary-field quantum Monte Carlo (QMC) techniques^{15,16} to study the ground state of the repulsive 2-D Hubbard model. Our goal was to shed light on the question of PS. A second motivation comes from ultra-cold atoms, where rapid experimental progress promises a new avenue — optical-lattice emulators¹⁷ — for direct “simulations” to investigate properties of Hubbard-like models. Detailed, accurate numerical data would allow quantitative benchmark and comparisons in future optical-lattice experiments. In our approach, the ability to control the sign/phase problem with a good approximation, combined with a boundary condition integration technique, drastically reduces the finite size and shell effects. This allows us to reach much higher accuracy than previously possible in the model. The measured equation

of state and spin-spin correlations, in lattice sizes up to 16×16 , show clear signals for PS at intermediate interaction strengths. The nature of this spatially inhomogeneous state is examined.

The Hamiltonian for the one-band Hubbard model is:

$$H = -t \sum_{\mathbf{j}, \delta, \sigma} \left(c_{\mathbf{j}, \sigma}^\dagger c_{\mathbf{j}+\delta, \sigma} + \text{h.c.} \right) + U \sum_{\mathbf{j}} n_{\mathbf{j}\uparrow} n_{\mathbf{j}\downarrow}, \quad (1)$$

where $c_{\mathbf{j}, \sigma}^\dagger$ ($c_{\mathbf{j}, \sigma}$) creates (annihilates) an electron with spin σ ($\sigma = \uparrow, \downarrow$) at lattice site \mathbf{j} , and δ connects two nearest-neighbor sites. The square lattice has size $N = L \times L$, with N_σ spin- σ electrons. The model has only two parameters, the strength of the interaction U/t (we will set $t = 1$) and the electron density $n \equiv (N_\uparrow + N_\downarrow)/N$.

PS occurs when the stability condition $\partial^2 e(n)/\partial n^2 > 0$ is violated, where $e(n)$ is the ground-state energy (per site) at density n . The critical value of n can be identified by Maxwell construction. Emery *et al.*⁶ showed that in the Hubbard (or t - J) model one could study

$$e_h(h) \equiv \frac{e(1-h) - e(1)}{h}, \quad (2)$$

where h is the hole density: $h \equiv 1 - n$. If PS exists, there is a minimum in $e_h(h)$ at h_c (or in the thermodynamic limit, a constant $e_h(h)$ for $h < h_c$)^{6,11}.

II. METHOD

A. Twist-Averaged Boundary Condition (TABC)

The signal for PS from Eq. (2) requires the slope of the equation of state, i.e., accurate numerical determination of small energy differences in the region where h is small. For a finite lattice, the shape of the Fermi surface varies considerably with n , which causes large variations in the energy. For example, with the usual periodic boundary condition (PBC), the smallest h accessible by a closed-shell system is ~ 0.15 in a 16×16 lattice¹⁸; even at 40×40 the finite-size effect is still sizable, especially in the region relevant for PS (see inset in Fig. 3). To reduce shell

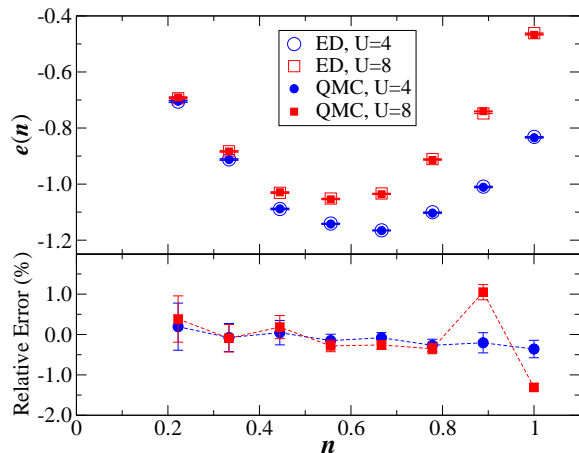


FIG. 1: (Color online) Upper panel: Ground state energy per site $e(n)$, versus density, of the 3×3 Hubbard lattice at $U = 4$ (blue) and 8 (red) calculated by ED (empty symbols) and our QMC method (filled symbols). At each density, the result is the average from 1000 random Θ values and the statistical error is estimated from their distribution. Bottom panel: Relative error (see text) of QMC ground state energy compared to the exact result (percentage).

and finite-size effects, we use twist-averaged boundary condition (TABC)^{19,20,21}, under which the wave function $\Psi(\mathbf{r}_1, \mathbf{r}_2, \dots)$ gains a phase when electrons hop around lattice boundaries:

$$\Psi(\dots, \mathbf{r}_j + \mathbf{L}, \dots) = e^{i\hat{\mathbf{L}} \cdot \Theta} \Psi(\dots, \mathbf{r}_j, \dots), \quad (3)$$

where $\hat{\mathbf{L}}$ is the unit vector along \mathbf{L} , and the twist angle $\Theta = (\theta_x, \theta_y)$ is a parameter. With a generic Θ , there will be no degeneracy in the one-electron energy levels. We average the results over many random twist angles²¹ in each system for convergence. As shown in Figs. 2 and 3, TABC essentially eliminates any shell effect. The disadvantage is that it turns the QMC sign problem¹⁵ into a phase problem¹⁶.

B. Constrained Path Monte Carlo under TABC

To treat this problem, we extend the constrained path Monte Carlo (CPMC) method¹⁵ to a Hamiltonian under TABC. For each given system (specified by N , n , U , and Θ), the method obtains a Monte Carlo (MC) representation of the many-body ground state $|\Psi_G\rangle$, by importance-sampled branching random walks (RWs)^{15,16} in the space of Slater determinant wave functions. The usual sign problem under PBC is caused by the symmetry^{15,22} between a Slater determinant $|\phi\rangle$ and a degenerate partner $-|\phi\rangle$ (exchanging two orbitals). To specify $|\Psi_G\rangle$, we need either, but not both. It can be shown^{15,23} that constraining the RWs to $\langle \Psi_G | \phi \rangle > 0$ is an exact boundary condition that eliminates the sign problem. In the constrained path approximation, a trial wave function $|\Psi_T\rangle$ is used in place of $|\Psi_G\rangle$.

Under TABC, the Slater determinants become complex, and we need to break the phase symmetry in $|\phi\rangle$. The Hubbard-Strotonovich transformation used in our calculations is the spin-decomposition of Hirsch²⁴, which results in *real* Ising-like auxiliary fields. The phase problem comes only from one-body hopping terms. We use a simple version of the phaseless approximation¹⁶ to constrain $|\phi\rangle$ to a unique phase. At each step of propagation, the paths of the RWs are required to satisfy:

$$\Re \left\{ \frac{\langle \Psi_T | \phi' \rangle}{\langle \Psi_T | \phi \rangle} \right\} > 0, \quad (4)$$

where $|\phi\rangle$ and $|\phi'\rangle$ are the current and proposed positions. The left-hand side is used in the importance sampling^{15,16,25}. We use the free-electron wave function as $|\Psi_T\rangle$. Since this is an eigenfunction of the complex kinetic energy terms of H , all the phase effect is absorbed in the *deterministic* one-body part. The condition on the RWs is equivalent to the original constrained path approximation¹⁵, to which Eq. (4) reduces if $\Theta = 0$. The phase constraint in Eq. (4) is the only approximation in our method.

Since the approximation involves only the overall sign/phase of the many-body wave function, it is reasonable to expect that the results will be relatively insensitive to $|\Psi_T\rangle$. Extensive benchmarks have shown this to be the case. The general approach has, in a variety of systems^{15,26,27,28}, given results among the most accurate that can be achieved presently from QMC.

As a quantitative measure in the current case, we compare $e(n)$ in 3×3 Hubbard lattices ($U = 4$ and 8) between our method (QMC) and exact diagonalization (ED). At each density (both $N_\uparrow = N_\downarrow$ and the polarized case $N_\uparrow - N_\downarrow = 1$, with $N_\downarrow = 1, 2, 3, 4$), we calculate the ground-state energies for 1000 random Θ values (identical in QMC and ED), average the results, and estimate a statistical error bar. In the QMC results, the error bar is the combined statistical errors from the random Θ distribution and the QMC sampling, although the latter is much smaller compared to the former in this system. The results are shown in Fig. 1. The agreement between QMC and exact results is excellent. The relative error $[e_{\text{QMC}}(n) - e_{\text{ED}}(n)]/|e_{\text{ED}}(n)|$, shown in the bottom panel, is essentially zero for $U = 4$ and is less than 1.5% for $U = 8$, across the entire density range.

III. RESULTS

A. Equation of state

Our main energy results are summarized in Fig.'s 2 and 3. In Fig. 2, the equation of state is presented for several lattice sizes and interaction strengths. For densities $n \lesssim 0.9$, convergence of the averaged energy is rapid with respect to the set of random twists, and typically 20 Θ 's is sufficient. For densities closer to half-filling,

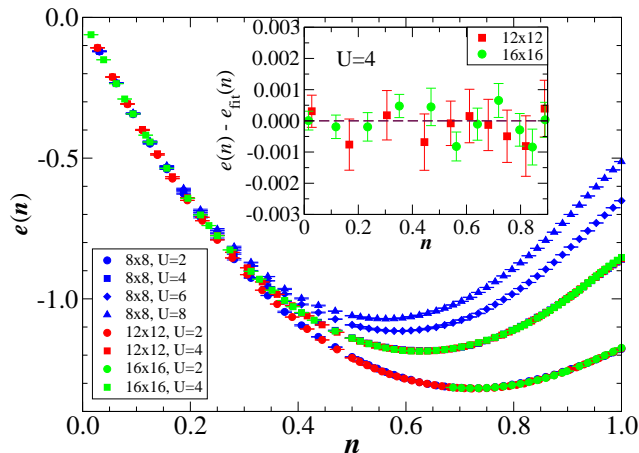


FIG. 2: (Color online) Ground state energy per site of the 2-D Hubbard model vs. density, for several interaction strengths and lattice sizes. Error bars are combined QMC and Θ -integration statistical errors. As a result of TABC, curves are smooth and different lattice sizes are indistinguishable. The inset shows convergence to the thermodynamic limit with a magnified view. (To reduce clutter, only every fifth density is shown for each size.) It also illustrates the accuracy of the fit $e_{\text{fit}}(n)$ across the density range for the phase below n_c .

the energy has stronger fluctuations with Θ . Further, the requirement on statistical accuracy is higher in this region, because the error bar on $e_h(h)$ is magnified by $1/h$ (see Eq. (2)). In this case, the number of boundary conditions is increased (to 60-300). In each region, the same set of random Θ values are used to help correlate the results at different densities. The main graph shows results from a Trotter time step $\Delta\tau = 0.05$; the fit below [Eq. (5)] and results in the inset have been extrapolated to $\Delta\tau = 0$. Convergence to the thermodynamic limit is seen with all three lattice sizes in the main graph. As the inset shows, 12×12 and 16×16 are indistinguishable to within statistical errors ($\sim 10^{-3}$).

In Fig. 3, the hole energy $e_h(h)$ derived from $e(n)$ is plotted. The inset illustrates the large finite-size and shell effects under the usual PBC. Because of degeneracies at the Fermi surface, the hole energy has kinks and is a constant below a finite hole concentration⁹. As the system size is increased, the $e_h(h)$ curves show convergence, but only slowly. Indeed a false signal for PS is seen in the non-interacting systems. These features are removed by TABC, with which a smooth monotonic curve is obtained. Excellent convergence toward the thermodynamic limit is achieved with a 12×12 lattice.

Interacting systems show similar behaviors: under PBC the same kinks appear in the $e(n)$ vs. n curves^{29,30} for the interaction strengths considered here. The combination of CPMC and TABC leads to a dramatic improvement. The main panel of Fig. 3 shows the hole energy for interacting systems. A clear minimum in $e_h(h)$ can be seen at a finite hole density in all cases when $U \geq 4$. At $U = 4$, h_c is ~ 0.07 - 0.1 . As U is increased, the position of the minimum is seen to shift to the right, i.e., to a larger

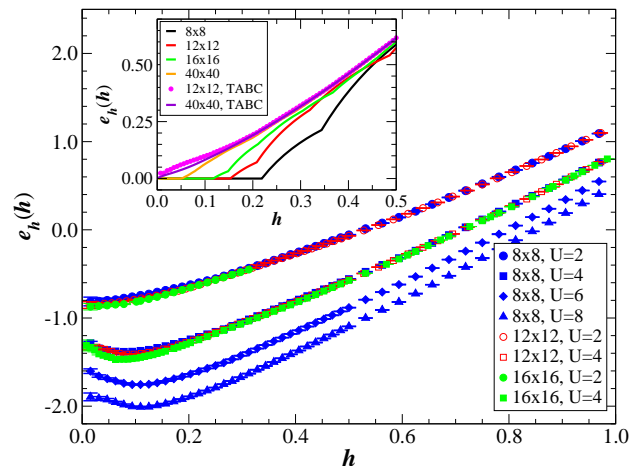


FIG. 3: (Color online) The hole energy $e_h(h)$ vs. hole density h for interacting systems, derived from Fig. 2. A clear minimum is seen for $U \geq 4$, at finite hole density h_c . The inset shows $e_h(h)$ for *non-interacting* Hubbard model calculated for lattices up to 40×40 with PBC. Note the kinks and the flat part of the curves near half-filling. The magenta curve is for a 12×12 lattice (and the dashed line, 40×40) using TABC, which effectively eliminates the finite-size and shell effects.

h_c . As U decreases to $U = 2$, $e_h(h)$ appears to decrease monotonically down to $h \sim 0.014$, the lowest doping in these lattices, although it cannot be completely ruled out a shallow (< 0.03 from $e_h(0)$) minimum exists within the statistical error bars.

The energy results indicate that, near half-filling, the system phase-separates into a hole-free phase of density $n = 1$ and a phase at $n_c = 1 - h_c$. Within a single phase, our results are expected to be at or near the thermodynamic limit. If the system is in a mixed state with two or more phases present, however, there are likely finite-size and/or interface effects. This appears to be the case from the data, where we see a minimum in the hole energy curves (as opposed to a flat region), as well as size variations in $e_h(h)$ in the hole density range $0 < h \lesssim h_c$. Similarly, if the system is in a spatially inhomogeneous spin or charge density wave state with very long wavelength modulations, for example a striplike state with only one stripe in a lattice of linear dimension up to $L \sim 16$, finite-size effects would likely make it indistinguishable from a phase-separated state in our calculations.

As a simple way to characterize the equation of state in the thermodynamic limit at $n < n_c$, we fit the calculated $e(n)$ on $n \in (0, 0.9)$ (size $L \geq 12$ only) to a 4-th order polynomial. For $U = 4$ this gives

$$e_{\text{fit}}(n) = -4.004n + 3.769n^2 - 0.700n^3 + 0.091n^4. \quad (5)$$

Statistical errors in the fitted coefficients are 10^{-3} to 10^{-2} . The inset in Fig. 2 shows the quality of the fit.

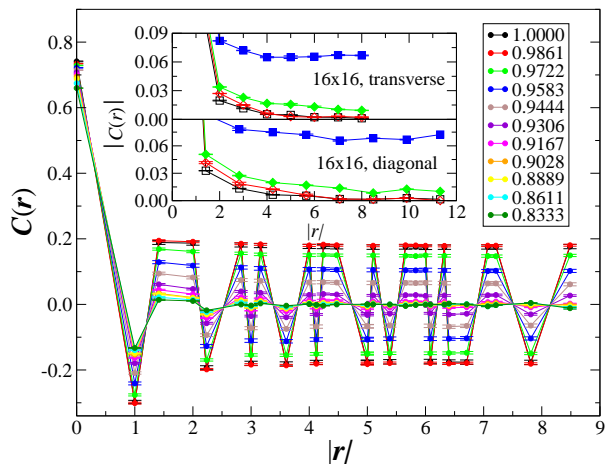


FIG. 4: (Color online) Spin-spin correlation function $C(\mathbf{r})$ for a 12×12 Hubbard lattice with $U = 4$. Within the PS region, the system exhibits long-range AF correlation. The strength of the long-range correlation decreases with doping, and vanishes at smaller densities. The inset shows a 16×16 lattice at $U = 4$, at a few selected densities near n_c : $n = 0.9688$ (blue square), 0.9453 (green diamond), 0.9297 (red empty diamond), and 0.9063 (black empty square). To aid the eye, the absolute value $|C(\mathbf{r})|$ is shown, along two separate directions. The behavior of the curves indicates the finite sizes of the AF phase in the periodic lattice.

B. Spin-Spin Correlation

At $n = 1$, the ground state is known to exhibit long-range antiferromagnetic (AF) order.^{24,31} Doping introduces frustration and tends to destroy the AF order. To see how this occurs and the relation to PS, we use the back-propagation technique^{15,25} to calculate the spin-spin correlation function:

$$C(\mathbf{r}) = \frac{1}{N} \sum_{\mathbf{j}} \langle (n_{\mathbf{j}+\mathbf{r},\uparrow} - n_{\mathbf{j}+\mathbf{r},\downarrow})(n_{\mathbf{j},\uparrow} - n_{\mathbf{j},\downarrow}) \rangle, \quad (6)$$

where \mathbf{r} is a vector on the lattice and $\langle \dots \rangle$ denotes expectation with respect to the ground state. The results for a 12×12 lattice at $U = 4$, after twist-averaging, are shown in Fig. 4. AF order is evident at $n = 1$, as expected. Note that the magnitude of the long-range part is ~ 0.2 , and double occupancy of \uparrow and \downarrow -electrons is significant, as the strength of the interaction U is moderate. The long-range order decays rapidly with n and, in the homogeneous phase, only short range correlation remains. (The minimum of $e_h(h)$ is around $n = 0.9167$ in 12×12 .)

A more quantitative picture can be seen from the spin structure factor: $S(\mathbf{q}) = \sum_{\mathbf{r}} C(\mathbf{r}) e^{i\mathbf{q}\cdot\mathbf{r}}$. When the system has AF order, $S(\mathbf{q})$ will peak at (π, π) . The calculated results are plotted in Fig. 5, as a function of n for three different lattice sizes. There is a marked difference between the small and larger doping regions. Below a critical density ($n \lesssim n_c$), $S(\pi, \pi)$ remains finite but is small and independent of lattice size, indicating the presence of short-range spin correlation but no long-range mag-

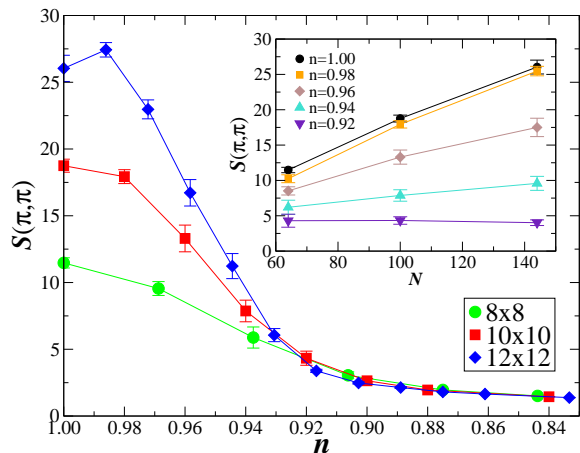


FIG. 5: (Color online) Spin structure factor at $\mathbf{q} = (\pi, \pi)$ for three system sizes calculated at $U = 4$. The lines are guides to the eye. The inset shows $S(\pi, \pi)$ vs. lattice size at several densities (obtained by linear interpolation if the exact n is not available in the particular lattice).

netic order. Beyond n_c , $S(\pi, \pi)$ increases quickly as n approaches 1. As the inset illustrates, at each density $S(\pi, \pi)$ grows proportionally with system size, suggesting the presence of long-range AF order.

We now further examine the spatial dependence of the spin correlation. From the Maxwell construction, the size of the AF region in a phase-separated system ($n > n_c$) is $N_{\text{AF}} = (1 - h/h_c)N$. In our calculations, $C(\mathbf{r})$ is averaged over imaginary-time and MC configurations. An AF cluster of linear dimension $l_{\text{AF}} > L/2$ should, due to “winding” around the periodic lattice, have a finite, constant tail $|C(\mathbf{r})|$ beyond $|\mathbf{r}| \sim L - l_{\text{AF}}$, while a smaller cluster should have a tail at zero beyond $|\mathbf{r}| \sim l_{\text{AF}}$. Our $C(\mathbf{r})$ results are consistent with this. In 12×12 , finite resolution gives only a handful of densities on the interval (n_c, n) , so l_{AF} is close to either L or 0 , and we see long plateaus. The inset in Fig. 4 shows 16×16 lattices, focusing on several densities near n_c . At $n = 0.9688$ and 0.9453 , $l_{\text{AF}} > L/2$, but the former (large l_{AF}) has a long flat tail while the latter shows a decline with $|\mathbf{r}|$ in the middle, indicating reduced contributions in the sum in Eq. (6). Similar effects are seen in the other pair ($l_{\text{AF}} < L/2$), with $n = 0.9297$ showing an extended intermediate region in which $|C(\mathbf{r})|$ is finite but decreasing, before the vanishing tail.

IV. DISCUSSION AND CONCLUSION

As we have discussed in Sec. II.B, our calculations use a non-perturbative, many-body QMC method. We return again to the only approximation in the method, namely the phase constraint, to help further gauge its impact. Although the possibility of a systematic bias cannot be ruled out, every indication has been that our results are very accurate — including the quality of the

present data, the consistency between the energy and spin correlation results, and the extensive benchmarks to date. As mentioned, the constrained path approximation has been tested (Refs. 15,23,30 and others) in various Hubbard systems under periodic or open boundary conditions. Accurate energy results are obtained. In realistic electronic systems, an approximation which is based on the same framework but which has to deal with a real two-body phase problem (as opposed to the non-stochastic one-body hopping phase here) has been benchmarked in molecules (Refs. 16,25,26,27 and others) against density-matrix renormalization group and quantum chemistry methods. Again the accuracy in the calculated ground state energy is consistent with that of Fig. 1.

In addition, several other factors in the present work provide more self-consistency checks and show the robustness of the results. At $n = 1$ and $U = 4$, an exact energy can be obtained with PBC: $e(1) = -0.8618(2)^{10,32}$, which is below our result: $-0.8559(4)^{33}$. Since our largest systematic error is expected to occur here (maximum n), this suggests that the tendency for PS would, if anything, be *underestimated* by our energies. Under TABC the entire density range (including half-filling) is treated with the same approach. All calculations use the corresponding free-electron wave function as $|\Psi_T\rangle$. An identical procedure is applied which has no tuning or adjustable parameters. Clearly the constraining $|\Psi_T\rangle$ has no minimum in e_h , but an unambiguous minimum emerges from the

calculations. Neither does $|\Psi_T\rangle$ contain spin order, but the AF ordering appears and vanishes, consistently with the behavior of the energy.

In summary, recent advances in QMC techniques have enabled us to determine the equation of state numerically in the 2-D Hubbard model at intermediate interactions. Our results show that, upon doping, the ground state separates into one phase with AF order (hole-free) and the rest without ($n_c \sim 0.92$ for $U = 4$). (The nature of the spatially inhomogeneous state will require further investigation, for example, the distinction between a phase-separated state in finite lattices and density waves with long wavelengths, as discussed in Sec. III.A. More calculations are on-going, which we plan to report in a future publication.) The size of the AF spin-density wave region vanishes at n_c , causing the system to lose long-range AF order.

V. ACKNOWLEDGEMENT

This work was supported by ARO (No. 48752PH). SZ also acknowledges support from NSF (DMR-0535592). We thank S. Sorella for sending us the 1/2-filling data, and E.J. Walter for help with computing. Computations were carried out at CPD and the SciClone Cluster (W&M), and at NCSA.

-
- ¹ J. Hubbard, Proc. R. Soc. London, A **276**, 283 (1963).
² P.W. Anderson, Science **235**, 1196 (1987).
³ E. Dagotto, Rev. Mod. Phys. **66**, 763 (1994).
⁴ D.J. Scalapino, J. Low Temp. Phys. **95**, 169 (2004).
⁵ J. M. Tranquada, B. J. Sternlieb, J. D. Axe, Y. Nakamura, and S. Uchida, Nature **375**, 561 (1995); M. Vershinin, S. Misra, S. Ono, Y. Abe, Y. Ando, and A. Yazdani, Science **303**, 1995 (2004); K. McElroy *et al.*, Phys. Rev. Lett. **94**, 197005 (2005).
⁶ V. J. Emery, S. A. Kivelson, and H. Q. Lin, Phys. Rev. Lett. **64**, 475 (1990).
⁷ C. S. Hellberg and E. Manousakis, Phys. Rev. Lett. **78**, 4609 (1997); Phys. Rev. B **61**, 11787 (2000).
⁸ A. Moreo and D. Scalapino, and E. Dagotto, Phys. Rev. B **43**, 11442 (1991).
⁹ H.Q. Lin, Phys. Rev. B **44**, 7151 (1991).
¹⁰ F. Becca, M. Capone, and S. Sorella, Phys. Rev. B **62**, 12700 (2000).
¹¹ A.C. Cosentini, M. Capone, L. Guidoni, and G. B. Bachelet, Phys. Rev. B **58**, R14685 (1998).
¹² R. Zitzler, Th. Pruschke, and R. Bulla, Eur. Phys. J. B **27**, 473 (2002).
¹³ A. Macridin, M. Jarrell, and Th. Maier, Phys. Rev. B **74**, 085104 (2006).
¹⁴ M. Aichhorn, E. Arrighoni, M. Potthoff, and W. Hanke, Phys. Rev. B **76**, 224509 (2007).
¹⁵ S. Zhang, J. Carlson, and J. E. Gubernatis, Phys. Rev. B **55**, 7464 (1997); J. Carlson, J. E. Gubernatis, G. Ortiz, and Shiwei Zhang, Phys. Rev. B **59**, 12788 (1999).
¹⁶ S. Zhang and H. Krakauer, Phys. Rev. Lett. **90**, 136401 (2003).
¹⁷ M. Lewenstein, A. Sanpera, V. Ahufinger, B. Damski, A. Sen, and U. Sen, Adv. Phys. **56**, 243 (2007).
¹⁸ A tilted lattice¹⁰ gives a closed-shell at a small h , but leaves a large gap before the next closed-shell filling.
¹⁹ D. Poilblanc, Phys. Rev. B **44**, 9562 (1991).
²⁰ C. Gros, Z. Phys. B - Condensed Matter **86**, 359 (1992); C. Gros, Phys. Rev. B **53**, 6865 (1996).
²¹ C. Lin, F. H. Zong, and D. M. Ceperley, Phys. Rev. E **64**, 016702 (2001).
²² S. Zhang and M. H. Kalos, Phys. Rev. Lett. **67**, 3074 (1991).
²³ Shiwei Zhang, Phys. Rev. Lett. **83**, 2777 (1999).
²⁴ J.E. Hirsch, Phys. Rev. B **31**, 4403 (1985).
²⁵ W. Purwanto and S. Zhang, Phys. Rev. E **70**, 056702 (2004); Phys. Rev. A **72**, 053610 (2005).
²⁶ W. A. Al-Saidi, Shiwei Zhang, and Henry Krakauer, J. Chem. Phys. **124**, 224101 (2006); *ibid.* **127**, 144101 (2007).
²⁷ M. Suewattana, Wirawan Purwanto, Shiwei Zhang, Henry Krakauer, and Eric J. Walter, Phys. Rev. B **75**, 245123 (2007).
²⁸ H. Kwee, Shiwei Zhang, and Henry Krakauer, Phys. Rev. Lett. **100**, 126404 (2008).
²⁹ N. Furukawa and H. Imada, J. Phys. Soc. Jpn. **61**, 3331 (1992).
³⁰ S. Zhang, J. Carlson and J. E. Gubernatis, Phys. Rev. Lett. **74**, 3652 (1995).
³¹ J.E. Hirsch and S. Tang, Phys. Rev. Lett. **62**, 591 (1989).

³² S. Sorella, private communication.

³³ Note that this is below what the fit in Eq. (5) *extrapolates*

to: $e_{\text{fit}}(1) = -0.844$, consistent with phase separation.